RSC Advances

PAPER

View Article Online
View Journal | View Issue

Cite this: *RSC Adv.*, 2018, **8**, 29295

A highly selective fluorescence "turn-on" sensor for Ca^{2+} based on diarylethene with a triazozoyl hydrazine unit†

Zhen Wang, Shiqiang Cui,* Shouyu Qiu and Shouzhi Pu*

A new photochromic diarylethene derivative with a triazozoyl hydrazine unit has been designed and synthesized. Its photochromism and photoswitchable fluorescence behaviors were studied systematically by the stimuli of lights and chemical substances in acetonitrile solution. With the addition of Ca^{2+}, the emission intensity enhanced 6.7 fold, accompanied by an obvious fluorescent color change from dark to light blue. The complexation between the derivative and Ca^{2+} is reversible with the 1 : 1 stoichiometry, which was verified by Job's plot and MS. The limit of detection (LOD) for Ca^{2+} was determined to be 2.49 $\times$ 10^{-8} mol L^{-1}. Based on this unimolecular platform, a logic circuit was designed with fluorescence intensity at 482 nm as the output and the combined stimuli of UV/vis and Ca^{2+}/EDTA as four inputs.

Received 16th July 2018
Accepted 10th August 2018

DOI: 10.1039/c8ra06039h

rsc.li/rsc-advances

Introduction

Calcium, the fifth most abundant element in the earth's crust, plays a very important role in many environmental and biological processes.[1–4] Meantime, Ca^{2+} is also a pivotal secondary messenger inside cells,[5–7] and visualization of Ca^{2+} intracellular dynamics has generated considerable biological knowledge.[8,9] Changes of Ca^{2+} concentration are related to immune responses and physiological responses to obesity.[10–17] High concentrations of Ca^{2+} ions will reduce the permeability of neuron membranes to sodium ions, thus reducing the excitability, resulting in low tension of smooth muscle.[18] Therefore, the effective and selective detection of Ca^{2+} ions is of great significance to medicine, environmental science and biochemistry.

Up to the present, there are a lot of traditional methods to detect various ions, such as atomic absorption spectrometry (AAS),[19] inductively coupled plasma mass spectrometry (ICP-MS),[20] voltammetry,[21] ion-selective membrane,[22] and liquid chromatography-mass spectrometry.[23] However, these methods all require high cost and complex instruments, and it is inconvenient to monitor the site quickly in different environments. Compared to these, a fluorescence probe is an effective tool to detect target ions due to its simplicity, easy implementation, high sensitivity and low detection limit.[24–31] To date, a number of fluorescent probes based on coumarin,[32] rhodamine,[33,34] nanoparticles,[35–37] polymeric phenols,[38,39] for the detection of Ca^{2+} have been reported. However, the Ca^{2+} selectivity of some probes is usually interfered by Mg^{2+} due to the similarly chemical behaviors of Ca^{2+} and Mg^{2+}. What's more, few of the reported detection capabilities have fluorescent "on–off" mode for the detection of Ca^{2+} or its fluorescence enhancement rate is very small. Hence, developing novel fluorescence probes with higher sensitivity and selectivity for Ca^{2+} is of the utmost importance at present.

Among the reported fluorescence probes, diarylethene derivatives are the most promising candidates, due to their excellent thermal stability, remarkable fatigue resistance, drug resistance and rapid response.[40–42] Furthermore, the identified ions could induce the diarylethene molecular to undergo polystable conversion,[43] and these properties make it possible for the application in the filed of multi-addressable switching. Although some of processes have been made in diarylethenes based on ion recognition,[44–50] the sensors for Ca^{2+} ions based on diarylethenes have rarely been reported.[51,52]

In this article, a new Ca^{2+} fluorescent sensor (**1o**) based on diarylethene and the triazozoyl hydrazine unit was designed and synthesized. The structure of **1o** was characterized by ^{1}H NMR, ^{13}C NMR, and HRMS, and the data were shown in ESI (Fig. S1–S3).† Its photochromism and fluorescent properties induced by lights and chemical species were also systematically discussed. The synthesis and photochromism of **1o** are shown in Scheme 1.

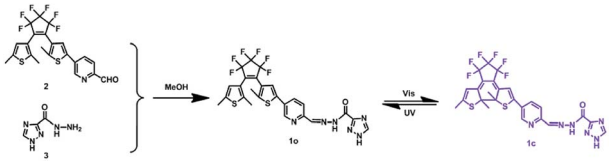

Scheme 1 The synthetic route and photochromism of **1o**.

Jiangxi Key Laboratory of Organic Chemistry, Jiangxi Science and Technology Normal University, Nanchang 330013, PR China. E-mail: cuisq2006@163.com; pushouzhi@tsinghua.org.cn; Fax: +86-791-83831996; Tel: +86-791-83831996

† Electronic supplementary information (ESI) available. See DOI: 10.1039/c8ra06039h

Experimental

General methods

Unless otherwise mentioned, all the reagents for the synthesis of the target compound were acquired from commercial suppliers and were used without further purification. All cations were added in the form of metal nitrates except for K^+, Sn^{2+} and Hg^{2+} (all of their counter ions were chloride ions). Metal ions solutions (0.1 mol L^{-1}) were prepared by dissolving their respective metal salts in deionized water. Necessary dilutions were made according to each experimental set up. NMR spectra were recorded on a Bruker AV400 spectrometer with deuterium generation of methanol (MeOD-d_4) and dimethylsulfoxide (DMSO-d_6) as solvents and tetramethylsilane (TMS) as an internal standard. Mass spectra were obtained using a Bruker Amazon SL ion trap mass spectrometer (ESI). The melting point was measured on a WRS-1B melting point apparatus. Absorption spectra were measured on an Agilent 8454 UV/vis spectrometer. Fluorescence spectra were recorded using a Hitachi F-4600 spectrophotometer. Photoirradiation was performed with an MUL-165 UV lamp and a MVL-210 visible lamp. Fluorescence quantum yield was measured with an Absolute PL Quantum Yield Spectrometer QYC11347-11.

Synthesis of 1o

Diarylethene **1o** was synthesized *via* the route shown in Scheme 1. Precursor **2** was synthesized according to the method reported in literature.[53] Then compound **2** (0.098 g, 0.2 mmol) was dissolved in 5.0 mL absolute methanol, followed by the addition of 1*H*-[1,2,4]triazole-3-carboxylic acid hydrazide (0.025 g, 0.2 mmol). The mixture was stirred for 12 h at room temperature in order to complete this reaction. After that, the solution was put into a refrigerator overnight. The crude product was washed with anhydrous methanol (5.0 mL × 3) and dried to give the bluish solid compound **1o** (0.081 g, yield: 68%) with the mp of 488–490 K. ^{1}H NMR (400 MHz, DMSO-d_6), δ (ppm): 1.86 (s, 3H), 1.95 (s, 3H), 2.41 (s, 3H), 6.84 (s, 1H), 7.72 (s, 1H), 8.00 (d, 1H, J = 7.8 Hz), 8.15 (d, 1H, J = 7.6 Hz), 8.60 (s, 1H), 8.81 (s, 1H), 8.90 (s, 1H), 12.35 (s, 1H), 14.70 (s, 1H). ^{13}C NMR (100 MHz, CH_3OD-d_4), δ (ppm): 11.6, 11.8, 12.1, 119.8, 122.7, 123.0, 123.3, 125.0, 125.3, 128.1, 129.0, 132.0, 132.4, 136.3, 137.1, 138.6, 142.0, 144.0, 147.4, 150.7. HRMS: m/z = 597.0943 $[M + H^+]^+$. Calcd 597.0968.

Results and discussion

Photochromism and fluorescent properties of 1o

The photochromic properties of **1o** were studied in acetonitrile (2.0×10^{-5} mol L^{-1}) at room temperature as shown in Fig. 1A. The absorption maximum of **1o** was observed at 343 nm ($\varepsilon = 4.4 \times 10^4$ mol^{-1} L cm^{-1}). Subsequently, upon irradiation with 297 nm light, a new broad absorption band centered at 572 nm ($\varepsilon = 1.2 \times 10^4$ mol^{-1} L cm^{-1}) emerged because of the formation of the closed-ring isomer **1c** with larger π-electron delocalization in the molecule.[54] In the photostationary state (PSS), a clear isosbestic point was observed at 365 nm, accompanied by a distinct color change from colorless to purple, which supported the reversible two-component photochromic reaction.[55] Conversely, upon irradiation with visible light (λ > 500 nm), the colored solution of **1c** was bleached entirely, and its absorption spectrum recovered to that of the open-ring isomer **1o**. The quantum yields of cyclization and cycloreversion were determined to be 0.24 and 0.022, with 1,2-bis(2-methyl-5-phenyl-3-thienyl)perfluorocyclopentene as a reference.[56] Additionally, the photochromic cyclization/cycloreversion kinetics were studied in acetonitrile solution (2.0×10^{-5} mol L^{-1}) at room temperature. As described in Fig. S4A,† the relationships between the absorbance and exposure time have good linearity upon irradiation with 297 nm light, suggesting that the cyclization processes of **1o** belong to the zeroth order reaction. The reaction rate constant (k_{o-c}) of **1o** was determined to be 1.51×10^{-3} s^{-1}. Similarly, the relationship between −log(Abs) and exposure time also has perfect linearity, indicating that the cycloreversion process belong to the first order reaction. The reaction rate constant (k_{c-o}) was determined to be 4.39×10^{-2} s^{-1} (Fig. S4B†). Furthermore, the fatigue resistance of **1o** was also studied by alternating UV and visible lights at room temperature (Fig. S5†). The results indicated that the coloration–decoloration cycles between **1o** and **1c** could be repeated for 10 times with 15% degradation.

Fig. 1B showed the fluorescence spectral changes of **1o** upon photoirradiation in acetonitrile solution (2.0×10^{-5} mol L^{-1}). The original state of **1o** displayed weak fluorescence at 443 nm

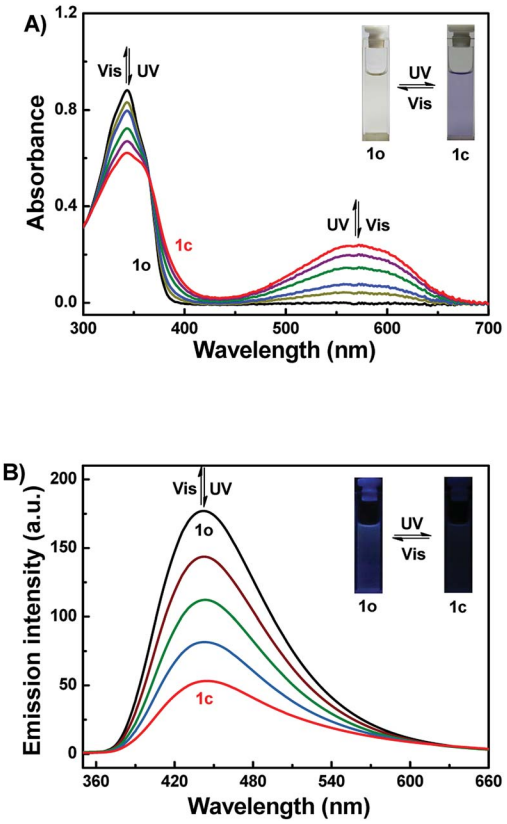

Fig. 1 Changes in the absorption (A) and fluorescence (B) spectra of **1o** upon irradiation with UV/vis lights in acetonitrile (2.0×10^{-5} mol L^{-1}) (λ_{ex} = 340 nm).

when excited at 340 nm, and the absolute fluorescence quantum yield was determined to be 0.005. On irradiation with 297 nm light, its emission intensity at 443 nm decreased gradually due to the generation of non-fluorescent isomer **1c**. When the PSS was reached, the emission intensity of **1o** was decreased significantly by *ca.* 70%, accompanied by the fluorescence color changed from dark purple to dark. Back irradiation with the proper wavelength of visible light ($\lambda > 500$ nm) regenerated the open-ring isomer **1o** and recovered the original state.

Fluorescence response to metal ions

Under the same experimental conditions, the fluorescence responses of **1o** toward various metal ions (5 equiv. 0.1 mol L^{-1}) were investigated in acetonitrile such as Al^{3+}, Cu^{2+}, Sn^{2+}, Zn^{2+}, K^{+}, Ag^{+}, Ni^{2+}, Ba^{2+}, Mg^{2+}, Mn^{2+}, Cd^{2+}, Sr^{2+}, Hg^{2+}, Co^{2+}, Cr^{3+}, Fe^{3+}, Pb^{2+} and Ca^{2+}. As can be seen in Fig. 2, when Ca^{2+} was added, the fluorescence intensity of **1o** was enhanced 6.7 fold as compared with the emission intensity of **1o** and the emission peak red shifted from 443 nm to 482 nm, accompanied by the fluorescent color change from dark purple to light blue. Furthermore, the fluorescence intensity of **1o** quenched with the addition of Cu^{2+}, Co^{2+}, Ni^{2+}. Moreover, upon addition of other metal ions, including Hg^{2+}, Mg^{2+}, Ca^{2+}, Ba^{2+}, Cr^{3+}, Al^{3+}, Mn^{2+}, Sr^{2+}, Pb^{2+}, Fe^{3+}, and K^{+}, the fluorescence spectra of **1o** showed inconspicuous changes. All the results indicated that the excellent capability of **1o** for distinguishing Ca^{2+} from other metals ions. Therefore, the diarylethene **1o** could be used as a selective fluorescence sensor for Ca^{2+} in acetonitrile.

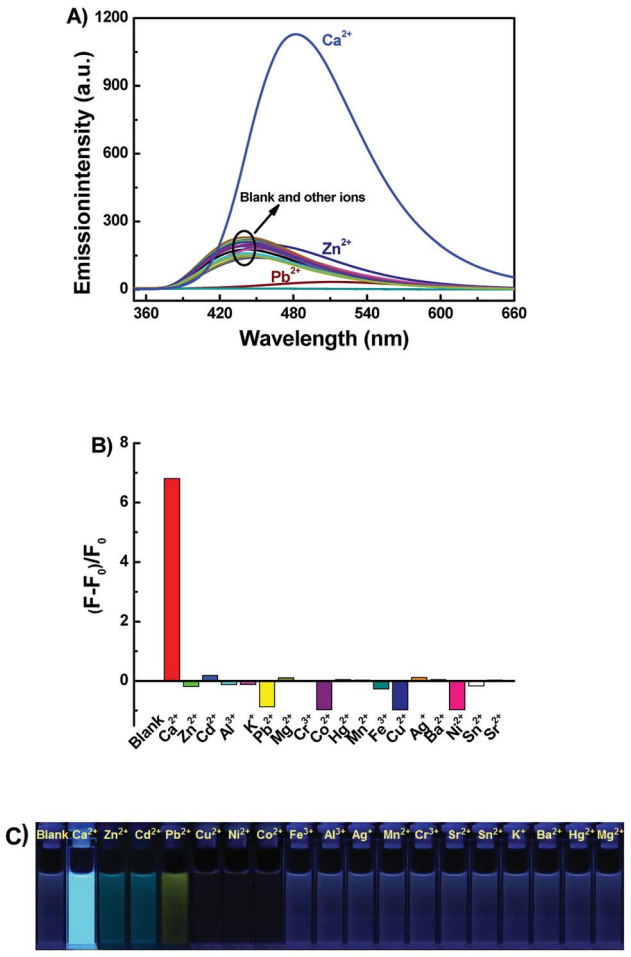

Fig. 2 Upon addition various metal ions to **1o** (2.0×10^{-5} mol L^{-1}) in acetonitrile: (A) fluorescence emission spectral changes ($\lambda_{ex} = 340$ nm); (B) emission intensity changes; (C) fluorescent photos.

Fluorescence studies of 1o toward Ca^{2+}

To further assess the responsive nature of **1o** induced by Ca^{2+}, the fluorescence spectral responses of **1o** toward Ca^{2+} in acetonitrile were investigated in Fig. 3A. The results turned out that sensor **1o** exhibited a very weak emission with a low quantum yield ($\Phi = 0.005$) at 340 nm excitation. With the gradual addition of Ca^{2+}, the emission intensity dramatically increased by 6.7 fold, accompanied by a red shift of 39 nm from 443 nm to 482 nm. Then the fluorescence intensity achieved its maximum until the amount of Ca^{2+} reached 2.2 equivalents of **1o** (Fig. S4†), and the absolute quantum yield of fluorescence was determined to be 0.03, which is 6 fold of **1o**. Meanwhile, the fluorescent color changed from dark purple to light blue, which was coincident with the changes in the fluorescence spectra. The weak fluorescence of the initial state **1o** was put down to the C=N isomerization, which has long been known as the dominant decay process.[57,58] However, a stable chelate **1o**–Ca^{2+} was

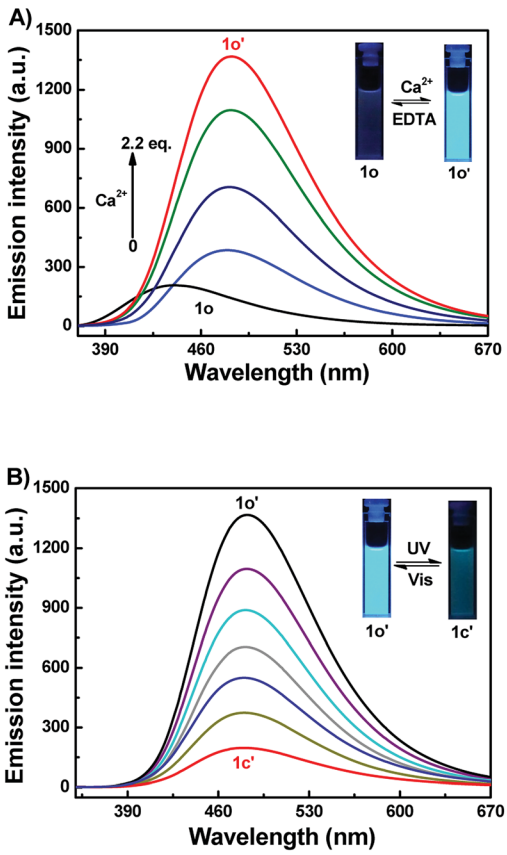

Fig. 3 (A) Fluorescence spectra changes of **1o** (2.0×10^{-5} mol L^{-1}) in acetonitrile induced by Ca^{2+} (0–2.2 equiv.); (B) fluorescence spectra changes of **1o′** (2.0×10^{-5} mol L^{-1} in acetonitrile), upon irradiation with UV-vis light ($\lambda_{ex} = 340$ nm).

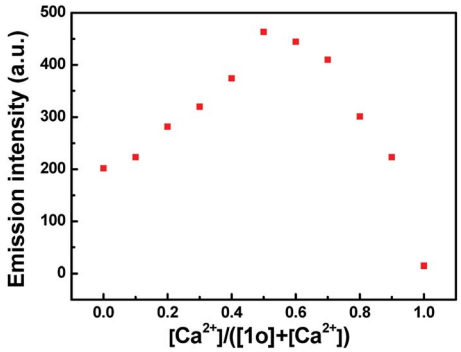

Fig. 4 Job's plot showing the 1 : 1 complex of **1o** and Ca^{2+} in acetonitrile (2.0×10^{-5} mol L^{-1}).

formed with the existence of Ca^{2+}. The isomerization of C=N bond was inhibited, which enhanced the rigidity of the molecule, thus leading to the chelation enhanced fluorescence (CHEF) effect.[59] Furthermore, the reversibility experiment was established by adding 6.0 equiv. EDTA (0.1 mol L^{-1}) to **1o**–Ca^{2+} (**1o′**) solution which possibly deprives Ca^{2+} away from the binding position. Eventually, the fluorescence spectrum of **1o′** was brought back to that of **1o**, suggesting that the complexation–decomplexation reaction between **1o** and Ca^{2+} was reversible.

Complexation mechanism of 1o with Ca^{2+}

To further investigate the coordination mode of **1o** and Ca^{2+}, Job's plot analysis was performed by using the emission intensity at 482 nm for Ca^{2+} as a function of molar fraction of **1o** according to the reported method.[60] As shown in Fig. 4, the maximum value was achieved when the molar fraction of $[Ca^{2+}]/([\mathbf{1o}] + [Ca^{2+}])$ was about 0.5, suggesting that **1o** was bound to Ca^{2+} with a 1 : 1 stoichiometry in acetonitrile. Based on these results and fluorescence titration data, the association constant (K_a) of **1o** with Ca^{2+} was calculated from the slope and intercept of these linear plots to be 8.86×10^3 L mol^{-1} with a good linear relationship ($R = 0.990$) (Fig. S6†). According to the method reported in previous literature,[61] the limit of detection (LOD) of **1o** toward Ca^{2+} was determined to be 2.49×10^{-8} mol L^{-1} (Fig. S7†). Therefore, **1o** could serve as a fluorescent sensor for detection of Ca^{2+} with high selectivity and sensitivity in acetonitrile.

^{1}H NMR titration experiments were also carried out in DMSO-d_6 to further study the binding mode of **1o** and Ca^{2+}. As shown in Fig. 5, the signals of the Ha (imino proton) at 12.48 ppm and the

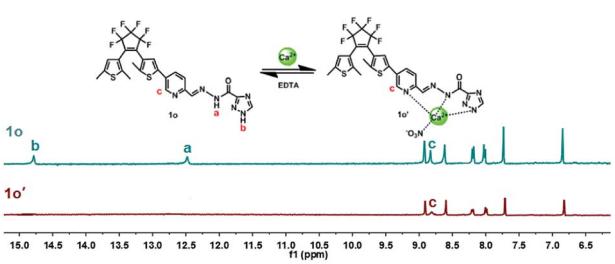

Fig. 5 Changes in ^{1}H NMR of **1o** and **1o′** in DMSO-d_6 (inset shows the proposed binding mode of **1o′** complex).

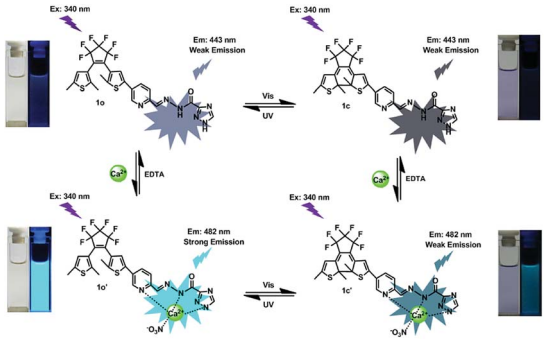

Scheme 2 Dual-controlled fluorescent switching behaviors of **1o** induced by Ca^{2+}/EDTA and UV/vis light.

Hb (–NH– proton on the triazole) at 14.70 ppm were found in the ^{1}H NMR spectrum of **1o**. With the addition of Ca^{2+}, the imino proton (Ha) disappeared completely, indicating the coordinate bond between imino N and Ca^{2+} was formed. Meanwhile, the –NH– proton (Hb) on the triazole was also disappeared finally, indicating that the formation of coordinate bond between the N atom on the triazole and Ca^{2+}. On the other hand, the signal of Hc on CH=N decreased gradually, and the Hc displayed a downfield shift of 0.01 ppm from 8.81 ppm to 8.82 ppm ultimately, showing that the formation of the coordinate bond between the N atom on the Schiff base and Ca^{2+}. All of the results suggested that the imino N, the N on the Schiff base unit, and the N on the triazole ring are the most reasonable binding sites. Furthermore, the HRMS analysis was also carried out to confirm the interaction between **1o**–Ca^{2+}. The testing sample was prepared by adding excessive Ca^{2+} to **1o** in acetonitrile, and the result displayed that the signal located at $m/z = 698.0362$ was consistent with the ensemble $[\mathbf{1o} + Ca^{2+} + NO_3^-]^+$ (m/z calcd: 698.0392) (Fig. S8†). These results further proved that **1o** and Ca^{2+} formed a 1 : 1 complex. Based on these facts, the most likely binding mode was shown in Scheme 2. Furthermore, the affection of pH to the sensor was also investigated. According to the methods in our previous work,[62] the fluorescence intensity changes of **1o** and **1o′** over different pH values in $CH_3CN : H_2O$ (9 : 1, v/v) were shown in Fig. S11.† The results demonstrated that the optimal pH region for sensor **1o** and **1o′** was 6.0–9.0.

Application in logic circuit and practical sample

According to the properties described above, the fluorescence emission of **1o** could be effectively modulated by either UV-vis

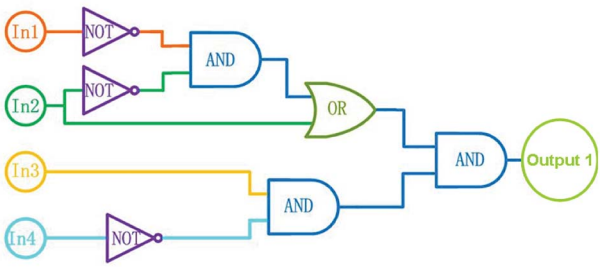

Fig. 6 Combinational logic circuits equivalent to the truth table given in Table 1: In1 (UV light), In2 (visible light), In3 (Ca^{2+}), In4 (EDTA).

Table 1 Truth table for all the possible strings of four binary-input data and the corresponding output digit

Inputs				Output[a]
In1 (UV)	In2 (Vis)	In3 (Ca^{2+})	In4 (EDTA)	(λ_{em} = 482 nm)
0	0	0	0	0
1	0	0	0	0
0	1	0	0	0
0	0	1	0	1
0	0	0	1	0
1	1	0	0	0
1	0	1	0	0
1	0	0	1	0
0	1	1	0	1
0	1	0	1	0
0	0	1	1	0
1	1	1	0	1
1	1	0	1	0
1	0	1	1	0
0	1	1	1	0
1	1	1	1	0

[a] At 482 nm, the emission intensity 6.7 fold of the original value is defined as 1, otherwise defined as 0.

lights or chemical reagents stimuli in acetonitrile, and the photoswitching behaviors of **1o** are shown in Scheme 2. On the basis of these facts, a logic circuit was constructed by using UV (In1), vis (In2), Ca^{2+} (In3), and EDTA (In4) as four input signals, and the emission intensity at 482 nm as the output signal (Fig. 6). The emission intensity of **1o** at 443 nm was considered as the initial value. When the emission intensity at 482 nm was 6.7 fold larger than the initial value, the output signal could serve as 'on' with a Boolean value of '1'. Otherwise, it serves as 'off' with a Boolean value of '0'. For instance, when the input strings were '1, 1, 1, and 0', the corresponding signals to In1, In2, In3, and In4 are 'on, on, on, and off'. Under this condition, **1o** was converted to **1o′** with the stimuli of Ca^{2+}, and the emission intensity increased dramatically. As a result, the output digital was '1'. Similarly, others stimuli would cause different on–off fluorescence switching. All of the possible logic strings were listed in the combinational logic circuit as shown in Table 1.

The application of **1o** to the practical samples was also performed. The Ca^{2+} content in real water samples from the Ganjiang River in Nanchang, Jiangxi province were determined. Table 2 displayed the results measured with **1o** after adding a moderate amount of Ca^{2+}. The recovery was ranged from 96.8% to 105%. These results indicated that **1o** could be used for detecting Ca^{2+} in practical samples with higher accuracy, and has certain practical value.

Table 2 Application in practical samples detection for Ca^{2+}

Sample	Ca^{2+} added (μM)	Ca^{2+} determined (μM)	Recovery (%)
1	0.40	0.42	105
2	0.80	0.81	101
3	1.20	1.18	98.3
4	1.60	1.55	96.8
5	2.00	1.97	98.5

Conclusions

In conclusion, a novel fluorescent sensor based on a diarylethene derivative with triazozoyl hydrazine unit was developed. The sensor exhibited high selectivity toward Ca^{2+} over other metal ions, and the detection limit for Ca^{2+} could be as low as 2.49×10^{-8} mol L^{-1}. Furthermore, a logic circuit was designed and constructed with the emission intensity at 482 nm as output signal and the UV/vis lights, Ca^{2+}/EDTA as input signals. The application results indicated that the sensor could be used for the detection of Ca^{2+} in practical samples. All these results will be helpful for the design and construction of new sensors for Ca^{2+} with high selectivity and sensitivity in the future.

Conflicts of interest

There are no conflicts to declare.

Acknowledgements

The authors are grateful for the financial support from the "5511" Science and Technology Innovation Talent Project of Jiangxi (2016BCB18015), the key project of Natural Science Foundation of Jiangxi Province (20171ACB20025), the Project of the Science Funds of the Education Office of Jiangxi (GJJ160773), the Young Talents Project of Jiangxi Science and Technology Normal University (2015QNBJRC004), the Project of Jiangxi Science and Technology Normal University Advantage Sci-Tech Innovative Team (2015CXTD002).

Notes and references

1 M. Landoni, B. F. Cerino, N. Haman, *et al.*, *J. Agric. Food Chem.*, 2013, **61**, 4622–4630.
2 S. M. Bawin and W. R. Adey, *Proc. Natl. Acad. Sci. U. S. A.*, 1976, **73**, 1999–2003.
3 S. V. Dorozhkin and M. Epple, *Angew. Chem., Int. Ed.*, 2002, **41**, 3130–3146.
4 S. Orrenius, B. Zhivotovsky and P. Nicotera, *Nat. Rev. Mol. Cell Biol.*, 2003, **4**, 552.
5 D. E. Clapham, *Cell*, 2007, **131**, 1047–1058.
6 E. Arunkumar, A. Ajayaghosh and J. Daub, *J. Am. Chem. Soc.*, 2005, **127**, 3156–3164.
7 T. Alizadeh, A. N. Shamkhali, Y. Hanifehpour, *et al.*, *New J. Chem.*, 2016, **40**, 8479–8487.
8 M. Raju, R. R. Nair, I. H. Raval, *et al.*, *Analyst*, 2015, **140**, 7799–7809.
9 Y. Nakagawa, Y. Watanabe, Y. Igarashi, *et al.*, *Bioorg. Med. Chem. Lett.*, 2015, **25**, 2963–2966.
10 A. T. Harootunian, J. P. Kao, S. Paranjape, *et al.*, *Science*, 1991, **251**, 75–78.
11 A. Minta, J. P. Kao and R. Y. Tsien, *J. Biol. Chem.*, 1989, **264**, 8171–8178.

12 G. Grynkiewicz, M. Poenie and R. Y. Tsien, *J. Biol. Chem.*, 1985, **260**, 3440–3450.
13 K. V. Kuchibhotla, C. R. Lattarulo, B. T. Hyman, *et al.*, *Science*, 2009, **323**, 1211–1215.
14 I. Micu, A. Ridsdale, L. Zhang, *et al.*, *Nat. Med.*, 2007, **13**, 874.
15 D. Skokos, G. Shakhar, R. Varma, *et al.*, *Nat. Immunol.*, 2007, **8**, 835.
16 J. Chambers, R. S. Ames, D. Bergsma, *et al.*, *Nature*, 1999, **400**, 261.
17 C. M. Armstrong and G. Cota, *Proc. Natl. Acad. Sci. U. S. A.*, 1999, **96**, 4154–4157.
18 M. Frankowski, A. Zioła-Frankowska and J. Siepak, *Talanta*, 2010, **80**, 2120–2126.
19 A. Sanz-Medel, A. B. S. Cabezuelo, R. Milačič, *et al.*, *Coord. Chem. Rev.*, 2002, **228**, 373–383.
20 R. N. Goyal, V. K. Gupta and S. Chatterjee, *Biosens. Bioelectron.*, 2009, **24**, 3562–3568.
21 V. K. Gupta, A. K. Singh, S. Mehtab, *et al.*, *Anal. Chim. Acta*, 2006, **566**, 5–10.
22 V. K. Gupta, R. Jain, S. Sharma, *et al.*, *Int. J. Electrochem. Sci.*, 2012, **7**, 569–587.
23 H. N. Kim, W. X. Ren, J. S. Kim, *et al.*, *Chem. Soc. Rev.*, 2012, **41**, 3210–3244.
24 Z. Shi, Y. Tu and S. Z. Pu, *RSC Adv.*, 2018, **8**, 6727–6732.
25 Y. L. Pak, K. M. K. Swamy and J. Yoon, *Sensors*, 2015, **15**, 24374–24396.
26 S. Pan, H. Tang, Z. Song, *et al.*, *Chin. J. Chem.*, 2017, **35**, 1263–1269.
27 M. Morimoto, Y. Takagi, K. Hioki, *et al.*, *Dyes Pigm.*, 2018, **153**, 144–149.
28 N. S. Wang, R. J. Wang, Y. Y. Tu, *et al.*, *Spectrochim. Acta, Part A*, 2018, **196**, 303–310.
29 N. Tetsuya, Y. Miyasaka and Y. Yokoyama, *Chem. Commun.*, 2018, **54**, 3207–3210.
30 C. Yu, L. Chen, J. Zhang, *et al.*, *Talanta*, 2011, **85**, 1627–1633.
31 C. Yu, J. Zhang, J. Li, *et al.*, *Microchim. Acta*, 2011, **174**, 247–255.
32 L. Cao, C. Jia, Y. Huang, *et al.*, *Tetrahedron Lett.*, 2014, **55**, 4062–4066.
33 X. Yu, P. Zhang, Q. Liu, *et al.*, *Mater. Sci. Eng., C*, 2014, **39**, 73–77.
34 M. S. Eom, W. Jang, Y. S. Lee, *et al.*, *Chem. Commun.*, 2012, **48**, 5566–5568.
35 J. Zhang, Y. Wang, X. Xu, *et al.*, *Analyst*, 2011, **136**, 3865–3868.
36 A. Ajayaghosh, E. Arunkumar and J. Daub, *Angew. Chem.*, 2002, **114**, 1844–1847.
37 S. K. Sharma, S. Kumar, R. Tyagi, *et al.*, *Microchem. J.*, 2008, **90**, 89–92.
38 R. Sahli, N. Raouafi, E. Maisonhaute, *et al.*, *Electrochim. Acta*, 2012, **63**, 228–231.
39 S. Z. Pu, T. S. Yang, J. K. Xu, *et al.*, *Tetrahedron*, 2005, **61**, 6623–6629.
40 S. Z. Pu, J. K. Xu, L. Shen, *et al.*, *Tetrahedron Lett.*, 2005, **46**, 871–875.
41 R. J. Wang, P. P. Ren, S. Z. Pu, *et al.*, *J. Photochem. Photobiol., A*, 2014, **294**, 44–53.
42 H. Tian, B. Qin, R. Yao, *et al.*, *Adv. Mater.*, 2003, **15**, 2104–2107.
43 Q. Zou, X. Li, J. Zhang, *et al.*, *Chem. Commun.*, 2012, **48**, 2095–2097.
44 A. Bianco, S. Perissinotto, M. Garbugli, *et al.*, *Laser Photonics Rev.*, 2011, **5**, 711–736.
45 Q. Zou, J. Jin, B. Xu, *et al.*, *Tetrahedron*, 2011, **67**, 915–921.
46 Z. Zhou, H. Yang, M. Shi, *et al.*, *ChemPhysChem*, 2007, **8**, 1289–1292.
47 Z. Zhou, S. Xiao, J. Xu, *et al.*, *Org. Lett.*, 2006, **8**, 3911–3914.
48 Z. Li, C. Zhang, Y. Ren, *et al.*, *Org. Lett.*, 2011, **13**, 6022–6025.
49 S. Z. Pu, D. Jiang, W. Liu, *et al.*, *J. Mater. Chem.*, 2012, **22**, 3517–3526.
50 R. Wang, X. Dong, G. Liu, *et al.*, *Luminescence*, 2015, **30**, 1290–1296.
51 S. Q. Cui, Z. Y. Tian, S. Z. Pu, *et al.*, *RSC Adv.*, 2016, **6**, 19957–19963.
52 S. Z. Pu, Z. P. Tong, G. Liu, *et al.*, *J. Mater. Chem. C*, 2013, **1**, 4726–4739.
53 M. Irie, *Chem. Rev.*, 2000, **100**, 1685–1716.
54 Z. X. Li, L. Y. Liao, W. Sun, *et al.*, *J. Phys. Chem. C*, 2008, **112**, 5190–5196.
55 S. Z. Pu, T. Yang, J. Xu, *et al.*, *Tetrahedron*, 2005, **61**, 6623–6629.
56 M. Irie, T. Lifka, S. Kobatake and N. Kato, *J. Am. Chem. Soc.*, 2000, **122**, 4871–4876.
57 W. K. Dong, X. L. Li, L. Wang, *et al.*, *Sens. Actuators, B*, 2016, **229**, 370–378.
58 E. T. Feng, Y. Y. Tu, C. B. Fan, *et al.*, *RSC Adv.*, 2017, **7**, 50188–50194.
59 Y. M. Xue, R. J. Wang, C. H. Zheng, *et al.*, *Tetrahedron Lett.*, 2016, **57**, 1877–1881.
60 W. Liu, L. Xu, R. Sheng, *et al.*, *Org. Lett.*, 2007, **9**, 3829–3832.
61 S. Guo, G. Liu, C. Fan, *et al.*, *Sens. Actuators, B*, 2018, **266**, 603–613.
62 Z. Wang, S. Q. Cui, S. Y. Qiu and S. Z. Pu, *Spectrochim. Acta, A*, 2018, **205**, 21–28.